A general criterion for viscoelastic secondary flow in pipes of noncircular cross section

Pengtao Yue

Department of Chemical and Biological Engineering, University of British Columbia, Vancouver, V6T 1Z3 BC, Canada and Department of Mathematics, University of British Columbia, Vancouver, V6T 1Z2 BC, Canada

Joseph Dooley

The Dow Chemical Company, 433 Building, Midland, Michigan 48667

James J. Feng[a)]

Department of Chemical and Biological Engineering, University of British Columbia, Vancouver, V6T 1Z3 BC, Canada and Department of Mathematics, University of British Columbia, Vancouver, V6T 1Z2 BC, Canada

(Received 6 August 2007; final revision received 19 October 2007)

Synopsis

This paper investigates the mechanism for secondary recirculations in non-Newtonian flows in a noncircular pipe, and develops a general criterion on the direction of the secondary flow based on the fluid rheology and the cross-sectional geometry of the pipe. Although the secondary flow is usually attributed to the second normal stress difference N_2, the relationship between the two turns out to be more involved than previously assumed. By theoretical analysis and numerical computations using the Giesekus model, we show that N_2 produces an effective body force that, if nonconservative, gives rise to secondary flows in the transverse direction. From this understanding, we propose a criterion for the direction of the secondary flow based on the second normal stress coefficient Ψ_2 and the shear viscosity η_s: if $\Psi_2(\dot{\gamma})/\eta_s(\dot{\gamma})$ is an increasing function of the strain rate $\dot{\gamma}$, the fluid flows from high shear regions to low shear regions along the walls and vice versa. This criterion accounts for all the prior computational work and resolves some inconsistencies in the literature. It is also consistent with all experimental observations to date. © *2008 The Society of Rheology.* [DOI: 10.1122/1.2817674]

I. INTRODUCTION

It is well known that non-Newtonian flows in a straight pipe of noncircular cross section are subject to secondary recirculations, with velocity components orthogonal to the primary axial flow. When the non-Newtonian fluid is sheared, it may experience two normal stress differences:

$$N_1(\dot{\gamma}) = \tau_{11} - \tau_{22} = \Psi_1(\dot{\gamma})\dot{\gamma}^2, \tag{1}$$

[a)]Author to whom correspondence should be addressed; electronic mail: jfeng@chml.ubc.ca

$$N_2(\dot{\gamma}) = \tau_{22} - \tau_{33} = \Psi_2(\dot{\gamma})\dot{\gamma}^2, \tag{2}$$

where $\dot{\gamma}$ is the shear rate and Ψ_1 and Ψ_2 are the first and second normal stress coefficients. Directions 1, 2, and 3 are the flow, velocity gradient and the neutral directions, respectively [Bird *et al.* (1987)]. The stress components in the transverse plane are ultimately responsible for the secondary flow, but geometry plays a key role as well, and no secondary flow occurs in a circular pipe. Hereafter, we will loosely speak of the normal stresses as representing fluid "elasticity", even though they actually stem from the nonlinearity of the constitutive equation and do not imply an elastic relaxation time. Although the magnitude of viscoelastic secondary flow is typically orders of magnitude lower than the primary flow, it may produce significant effects by introducing flow across the otherwise rectilinear streamlines. For example, it is known to greatly enhance heat transfer in pipe flows [Gao and Hartnett (1996); Syrjälä (1998)]. In bicomponent coextrusion, secondary flows produce considerable interface deformation over an axial distance $\sim 100D$, D being the characteristic dimension of the cross section [Debbaut *et al.* (1997); Dooley *et al.* (1998); Debbaut and Dooley (1999); Dooley (2002); Dooley and Rudolph (2003)]. In multilayer film extrusion, such interfacial distortion leads to nonuniform layer thickness and poor product quality.

Owing to its fundamental and practical importance, secondary flow of non-Newtonian fluids in noncircular pipes has received numerous investigations since the 1950's. Despite the effort, the physical mechanism remains somewhat unclear, and there is no universal criterion that specifies the direction of the secondary flow based on the fluid rheology and flow geometry. Experimentally, several groups have observed secondary flows of polymer solutions and melts in pipes of elliptic [Giesekus (1965)] and square cross sections [Dodson *et al.* (1974); Townsend *et al.* (1976); Debbaut *et al.* (1997); Dooley *et al.* (1998); Dooley (2002); Dooley and Rudolph (2003)]. In all cases, the direction of the secondary flow is such as to go from areas of high shear to low shear along the wall. For an elliptic cross section, four recirculating eddies occupy the four symmetric quadrants, flowing from the center toward the wall along the minor axis and back to the center along the major axis. For a square cross section, eight eddies are demarcated by the symmetry lines, going from the center of the sides toward the corners. Theoretically and computationally, a larger number of studies have been devoted to secondary flows in those geometries using different constitutive models, including Reiner–Rivlin [Green and Rivlin (1956); Gao and Hartnett (1993, 1996); Hashemabadi and Etemad (2006)], Criminale–Ericksen–Filbey (CEF) [Dodson *et al.* (1974); Townsend *et al.* (1976); Gervang and Larsen (1991); Syrjälä (1998); Mai–Duy and Tanner (2005)], corotational Maxwell [Thangam and Speziale (1987)], Phan–Thien–Tanner (PTT) [Tanoue *et al.* (2006)], modified PTT (MPTT) [Xue *et al.* (1995)], Giesekus [Debbaut *et al.* (1997);Debbaut and Dooley (1999)], and Leonov [Siline and Leonov (2001)]. For square and elliptic cross sections, all predict the correct number of eddies and the general flow pattern. However, there has been much confusion over how the direction of the recirculation depends on fluid rheology.

It can be easily shown that N_1 has no contribution to the traction acting in the transverse plane, and N_2 is the driving mechanism of secondary flow (see the Appendix for a proof). Thus, most prior studies have focused on N_2 or Ψ_2. Calculations based on the Reiner–Rivlin [Gao and Hartnett (1993, 1996); Hashemabadi and Etemad (2006)] and CEF [Dodson *et al.* (1974)] models suggest that the correct sense of recirculation can be produced only by employing a positive Ψ_2. But it is well known that polymer solutions and melts possess a negative second normal stress difference with which the secondary flow would be predicted in the wrong direction, i.e., going from the corner toward the

center of the sides in a square pipe. A clue to this puzzle lies in an earlier analysis by Oldroyd (1965), which showed that for any viscoelastic fluid, no secondary flow can arise if the ratio between Ψ_2 and the steady shear viscosity η_s is a constant, independent of the strain rate $\dot{\gamma}$. In other words, one may add a constant multiple of η_s to Ψ_2 without affecting the secondary flow. Hence, there can be no general correlation between the secondary flow and the magnitude or sign of Ψ_2; an attempt at such a correlation is necessarily restricted to the specific model that happens to predict a certain Ψ_2. This insight was later corroborated by Townsend *et al.* (1976), who varied the coefficients of the CEF model to tune the functional form of Ψ_2 and concluded that the direction of secondary flow does not correlate with the sign of Ψ_2. More recent calculations using CEF and rate-type viscoelastic models have also confirmed that no secondary flow occurs if Ψ_2/η_s is a constant [Xue *et al.* (1995); Gervang and Larsen (1991); Syrjälä (1998)].

So far, the most general criterion on the secondary flow in a square pipe is due to Syrjälä (1998) using the CEF model. Assuming power laws for the shear viscosity and second normal stress coefficient: $\eta_s \propto \dot{\gamma}^{n-1}$ and $\Psi_2 = c\dot{\gamma}^m$, c being a constant, Syrjälä computed the secondary flow using series of m, n, and c values. The numerical results are such that the secondary flow goes from the center of the sides toward the corners if $[m-(n-1)]c>0$, and in the opposite direction if $[m-(n-1)]c<0$. This empirical criterion is consistent with Oldroyd's condition [Oldroyd (1965)] as well as prior computations based on power-law functions for Ψ_2 and η_s [Gao and Hartnett (1993, 1996); Hashemabadi and Etemad (2006)]. It is unclear whether a similar criterion applies to the CEF model with more general material functions, or even to the more general rate-type constitutive models. Numerical calculations based on the PTT [Tanoue *et al.* (2006)], MPTT [Xue *et al.* (1995)] and Giesekus [Debbaut *et al.* (1997); Debbaut and Dooley (1999)] models predict the correct secondary flow direction using a negative Ψ_2. However their relationship to the Syrjälä criterion cannot be ascertained since η_s and Ψ_2 cannot be cast into power laws. Is there a common principle underlying all the calculations? Is there a universal criterion that works for all the viscoelastic models? These questions have motivated the present work.

We use theoretical analysis and numerical computations to develop a general criterion for the direction of secondary flows based on the fluid rheology and the cross-sectional geometry. In this process, we elucidate the mechanism for the secondary flow, which turns out to be more involved than N_2 or Ψ_2. The criterion is shown to account for all prior results and resolves the apparent contradictions in the literature.

II. PROBLEM SETUP AND NUMERICAL METHOD

Following prior work on viscoelastic secondary flows [Xue *et al.* (1995); Debbaut *et al.* (1997); Tanoue *et al.* (2006)], we consider the fully developed flow of a viscoelastic fluid in a conduit of noncircular cross section, schematically shown in Fig. 1. The primary flow, along the z direction, is driven by a constant pressure gradient, and all the other variables do not depend on z. This setup retains three-dimensional (3D) components of the flow and stress fields, but the solution is done in the two-dimensional (2D) domain Ω.

The theoretical analysis will be for a general non-Newtonian fluid, but the numerical computations are for a Giesekus fluid. In the latter case, the governing equations are

$$\nabla \cdot \boldsymbol{v} = 0, \tag{3}$$

$$\rho\left(\frac{\partial \boldsymbol{v}}{\partial t} + \boldsymbol{v}\cdot\nabla\boldsymbol{v}\right) = -\nabla p + \mu_s\nabla^2\boldsymbol{v} + \nabla\cdot\boldsymbol{\tau}_p, \tag{4}$$

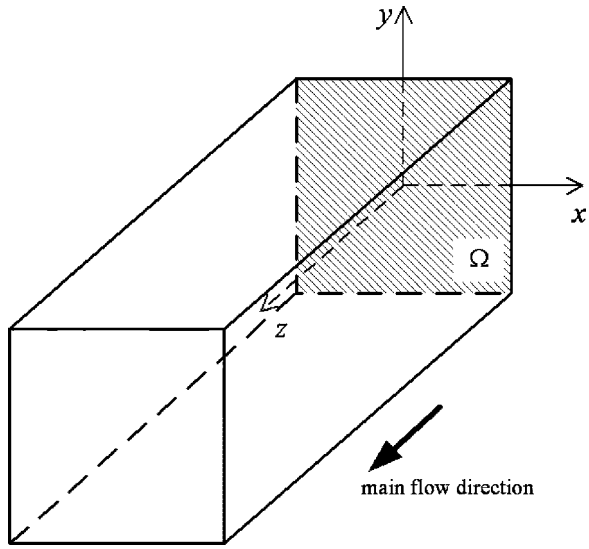

FIG. 1. Schematic of the flow geometry.

$$\boldsymbol{\tau}_p + \lambda_H \boldsymbol{\tau}_{p(1)} + \alpha \frac{\lambda_H}{\mu_p}(\boldsymbol{\tau}_p \cdot \boldsymbol{\tau}_p) = \mu_p[\nabla \boldsymbol{v} + (\nabla \boldsymbol{v})^{\mathrm{T}}], \tag{5}$$

where μ_s, μ_p, $\boldsymbol{\tau}_p$, λ_H, and α are the solvent viscosity, polymer viscosity, polymer stress tensor, polymer relaxation time, and mobility parameter in the Giesekus model. The subscript $_{(1)}$ denotes the upper convected derivative.

The problem is made dimensionless by using the characteristic size of the cross section D, the total viscosity of the fluid $\mu = \mu_s + \mu_p$, and the average axial velocity of the primary flow W. This leads to the following dimensionless groups:

$$Re = \frac{\rho W D}{\mu} \quad \text{(Reynolds number)},$$

$$De = \frac{\lambda_H W}{D} \quad \text{(Deborah number)}, \tag{6}$$

$$\beta = \frac{\mu_s}{\mu} \quad \text{(retardation} - \text{relaxation time ratio)},$$

plus the mobility parameter of the Giesekus fluids α, and geometric ratios characterizing the cross section Ω. In polymer extrusion experiments, $\rho \sim 1$ g/cm^3, $\mu \sim 10^4$ poise, $W \sim 1$ cm/s, $D \sim 1$ cm [Debbaut *et al.* (1997)]. Thus $Re \sim 10^{-4}$ and inertia is negligible. In our simulations, we have set Re to zero.

The governing equations are solved by a finite-element code AMPHI [Yue *et al.* (2006b)], originally developed for two-component complex fluids but used here for a single fluid. The domain Ω is discretized by an unstructured triangular mesh; P2 elements are used for $\boldsymbol{v}$ and P1 elements for p and $\boldsymbol{\tau}_p$. Second-order implicit schemes are used for temporal discretization. The code has been extensively validated in the past [Yue *et al.* (2006b, 2006a)]. For the geometry at hand, we have calculated the pressure driven flow of a Newtonian fluid in a rectangular pipe of $4D \times 1D$, and the axial velocity profiles are

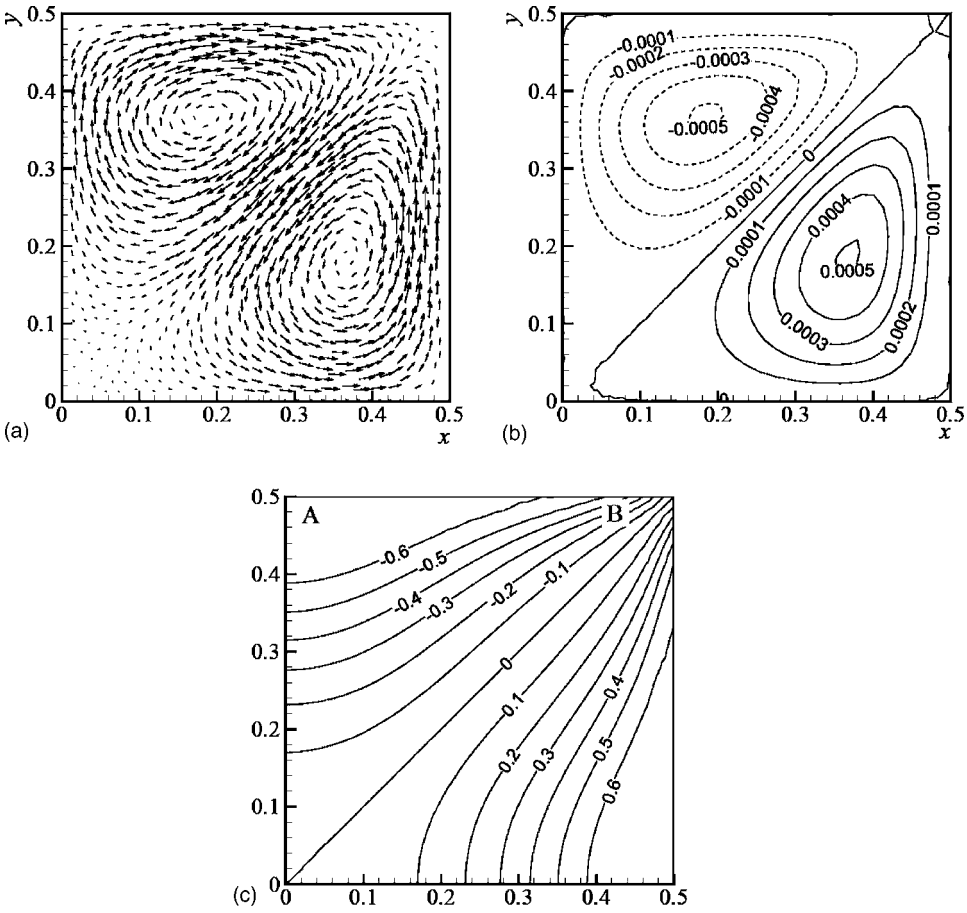

FIG. 2. The secondary flow in the upper right quadrant of the square cross section for a Giesekus fluid. (a) Velocity vectors (u,v); (b) contours of the stream function ψ; (c) contours of the polymer normal stress difference $\tau_{pyy}-\tau_{pxx}$. $De=1$, $\alpha=0.5$, $\beta=0.1$.

compared with a finite difference solution to the corresponding Poisson equation on a dense Cartesian mesh of 800×200. A coarse mesh with grid size $h=0.1D$ already produces accurate results. However, to guarantee the resolution of the secondary flows in viscoelastic fluids, we have used a more conservative value $h=0.02D$ for all simulations in the rest of paper.

III. RESULTS AND DISCUSSION

A. Secondary flow in square cross section

The square cross section is the most common geometry in the literature on viscoelastic secondary flows [Xue *et al.* (1995); Debbaut and Dooley (1999); Tanoue *et al.* (2006)]. In this subsection, we briefly illustrate the main features of the secondary flow of a Giesekus fluid in a square pipe and point out their apparent connection to N_2. This prefaces an analysis of the mechanism of the secondary flow in the next subsection, which is the main result of the paper.

Figure 2 depicts the velocity and stress fields for the secondary flow. The flow pattern is the same as reported in the literature for other constitutive models [e.g., Townsend *et*

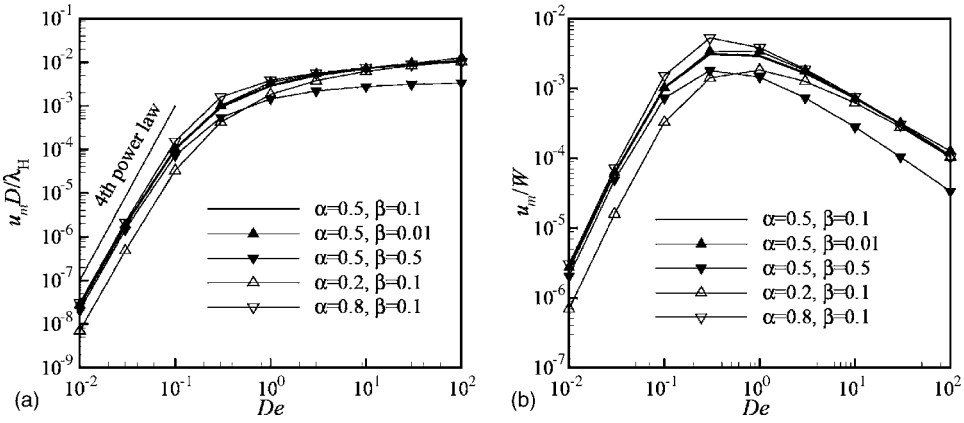

FIG. 3. The magnitude of secondary flow as a function of De. u_m is the average of $\sqrt{u^2+v^2}$ over the cross section.

al. (1976); Xue *et al.* (1995); Gao and Hartnett (1996); Debbaut *et al.* (1997); Debbaut and Dooley (1999)]. Due to symmetry, there are two counter rotating vortices in each quarter, and near the wall, the fluid flows from the center of the wall to the corner. Based on the velocity components u and v, we can define a stream function ψ by $u=\partial\psi/\partial y$ and $v=-\partial\psi/\partial x$, which is shown in Fig. 2(b). A positive ψ value indicates counterclockwise rotation and a negative value denotes the reverse. These are depicted respectively by solid and broken contours, and the same convention is used for contour plots hereafter. Figure 2(c) shows contours of the polymer normal stress difference $\tau_{pyy}-\tau_{pxx}$. As the direction of the velocity gradient ∇w varies over the cross section, $\tau_{pyy}-\tau_{pxx}$ does not coincide with N_2 as defined in Eq. (2), except near the upper wall. Nevertheless, it is clear that the polymer is more severely sheared near the center of the walls (point A) than near the corner (point B).

More quantitatively, the magnitude of the recirculation can be represented by the average velocity $u_m=\frac{1}{A}\int_\Omega\sqrt{u^2+v^2}d\Omega$, A being the area of Ω. Figure 3 plots u_m as a function of the Deborah number De. For vanishing De, u_m approaches zero with the scaling $u_m\propto De^4$, as has been previously reported [Xue *et al.* (1995); Debbaut and Dooley (1999)]. As De increases beyond unity, u_m tends to level off, indicating a finite limiting value as $De\to\infty$. This asymptotic behavior may have interesting practical implications. The ratio u_m/W increases with De first, reaches a maximum around $De=1$, and then declines as $1/De$ for higher De [Fig. 3(b)]. Thus, to strike a balance between raising production rate and minimizing distortion due to secondary flow, faster flows are advantageous over slower ones. We have also explored moderate ranges of the mobility parameter α and the retardation time via β. The general trend is that u_m increases with α and decreases with β, but their effects on u_m are minor.

The $u_m(De)$ curves mirror the variation of N_2 with the shear rate $\dot\gamma$ for a Giesekus fluid in simple shear [Isaki and Takahashi (2002)], which is plotted in Fig. 4. The variations with respect to α and β also show close correspondence between u_m and N_2. In the limits of small and large De, N_2 has the following asymptotic formulas: $N_2=-\alpha(1-\beta)\mu\lambda_H\dot\gamma^2$ for small De; $N_2=-(1-\beta)\mu/\lambda_H$ for large De [Bird *et al.* (1987)]. Note that N_2 levels off for large De because of shear thinning in the Giesekus model, and no longer depends on $\dot\gamma$ for sufficiently fast flows. However, for small De, $N_2\propto De^2$ while $u_m\propto De^4$. Thus, even though N_2 is the driving force of the secondary flow, the relationship between the two is

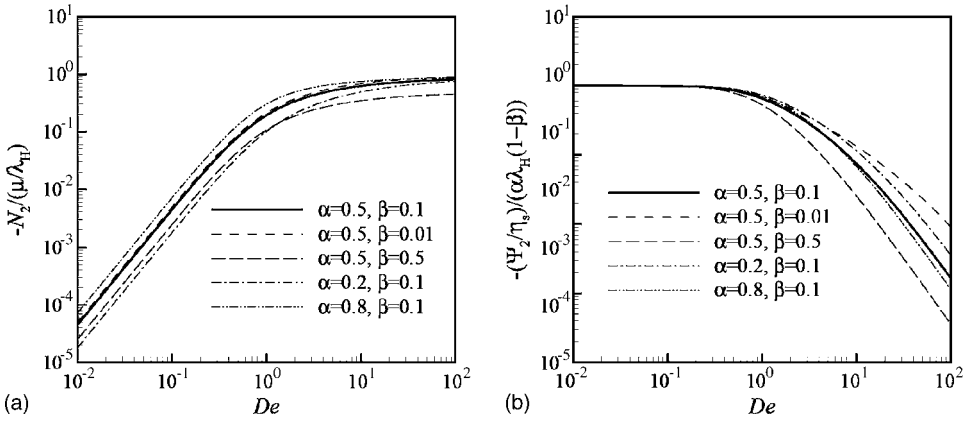

FIG. 4. The second normal stress difference of a Giesekus fluid in simple shear of shear rate $\dot{\gamma}$. (a) $-N_2$ normalized by μ/λ_H; (b) the function $-\Psi_2/\eta_s$, normalized by $\alpha(1-\beta)\lambda_H$, which is significant in analyzing the origin of the secondary flow in the next subsection. Note that the Deborah number $De=\lambda_H\dot{\gamma}$ is different from the definition in the pipe flow [Eq. (6)].

not straightforward. This point may be more qualitatively argued using Fig. 2(c). Near the upper wall the flow becomes planar shear and $\tau_{pyy}-\tau_{pxx}$ approximates N_2. The negative N_2 may be seen as a tension in the neutral direction (i.e., the x direction). Since this tension is higher at point A than B, one might naively expect the fluid to be dragged from the corner toward the center of the wall. The actual recirculation goes in the opposite direction, and its genesis requires a more refined explanation, to be sought in the next subsection.

B. Mechanism of secondary flow

Under the assumptions of fully developed flow and vanishing inertia, the x and y components of the momentum equation [Eq. (4)] can be written as

$$0=-\nabla p+\mu_s\nabla^2\boldsymbol{v}+\nabla\cdot\boldsymbol{\tau}_p, \tag{7}$$

where $\nabla=(\partial/\partial x,\partial/\partial y)$, and $\boldsymbol{v}=(u,v)$ and

$$\boldsymbol{\tau}_p=\begin{pmatrix}\tau_{xx} & \tau_{xy}\\ \tau_{yx} & \tau_{yy}\end{pmatrix} \tag{8}$$

now denote the 2D velocity vector and polymer stress tensor on the x-y plane. It is clear that the polymer stress drives the secondary flow, with the pressure p serving as a Lagrange multiplier to satisfy the continuity equation. To estimate the polymer stress $\boldsymbol{\tau}_p$, let us temporarily neglect the secondary flow and consider the rectilinear flow $w(x,y)$. This is permissible since u and v are typically much smaller than w and can be treated as perturbations on the primary flow [Tanner (2000)]. Now $w(x,y)$ constitutes a viscometric flow whose strain rate and gradient direction vary spatially. At each point (x,y), the direction along ∇w is designated by coordinate x_2 and the orthogonal neutral direction by x_3 in keeping with the subscript convention for the normal stress differences in Eqs. (1) and (2). In the local Cartesian frame (x_2,x_3) as shown in Fig. 5, the polymer stress tensor is diagonal since in-plane shearing due to (u,v) is negligible:

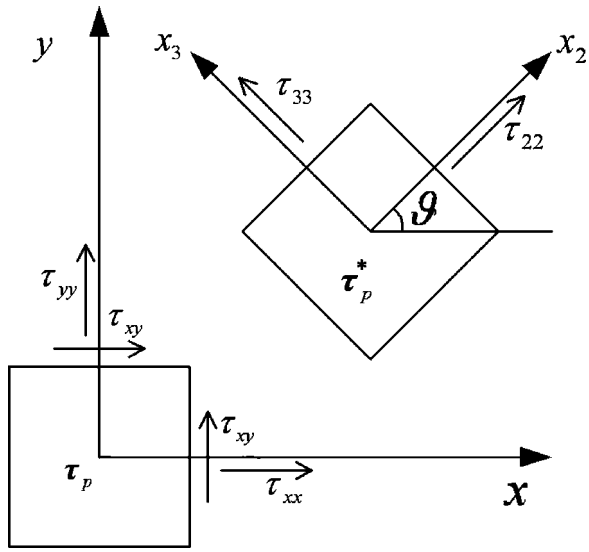

FIG. 5. Schematic of the (x,y) and (x_2,x_3) coordinate systems.

$$\boldsymbol{\tau}_p^* = \begin{pmatrix} \tau_{22} & 0 \\ 0 & \tau_{33} \end{pmatrix} = \tau_{33}\boldsymbol{I} + \begin{pmatrix} \Psi_2(\dot{\gamma})\dot{\gamma}^2 & 0 \\ 0 & 0 \end{pmatrix}. \tag{9}$$

In the previous $\boldsymbol{I}$ is the 2D isotropic tensor and $\dot{\gamma}=\sqrt{w_x^2+w_y^2}$ is the shear rate, with subscripts $_x$ and $_y$ denoting derivatives with respect to x and y. Rotating back to the (x,y) frame, the polymer stress is

$$\boldsymbol{\tau}_p = \boldsymbol{R}\cdot\boldsymbol{\tau}_p^*\cdot\boldsymbol{R}^{\mathrm{T}} = \tau_{33}\boldsymbol{I} + \begin{pmatrix} \Psi_2 w_x^2 & \Psi_2 w_x w_y \\ \Psi_2 w_x w_y & \Psi_2 w_y^2 \end{pmatrix}, \tag{10}$$

where the rotation matrix $\boldsymbol{R}$,

$$\boldsymbol{R} = \begin{pmatrix} \cos\vartheta & -\sin\vartheta \\ \sin\vartheta & \cos\vartheta \end{pmatrix}, \tag{11}$$

is defined by the angle ϑ between the gradient direction ∇w and the x axis. In view of Eq. (10), the momentum equation [Eq. (7)] can be rearranged as

$$0 = -\nabla\tilde{p} + \mu_s\nabla^2\boldsymbol{v} + \boldsymbol{f}, \tag{12}$$

where $\tilde{p}=p-\tau_{33}$, and $\boldsymbol{f}$ is the body force due to the polymer stress

$$\boldsymbol{f} = \nabla\cdot(\boldsymbol{\tau}_p - \tau_{33}\boldsymbol{I}) = \nabla\cdot\begin{pmatrix} \Psi_2 w_x^2 & \Psi_2 w_x w_y \\ \Psi_2 w_x w_y & \Psi_2 w_y^2 \end{pmatrix}. \tag{13}$$

The momentum equation in the z direction is

$$0 = -p_z + \nabla\cdot(\eta_s(\dot{\gamma})\nabla w), \tag{14}$$

where $\eta_s(\dot{\gamma})$ is the steady shear viscosity measured in simple shear, and $p_z<0$ is the constant pressure gradient that drives the axial flow.

Thus the secondary flow (u,v) can be viewed as a 2D viscous flow driven by $\boldsymbol{f}$, which is due to the second normal stress difference produced by the shear in the axial primary

flow. If $\boldsymbol{f}$ is conservative, i.e., $C=\nabla\times\boldsymbol{f}=0$, work done by $\boldsymbol{f}$ along any closed loop is nil. Then no secondary flow could be sustained and will be eventually dissipated. $C>0$ drives a counterclockwise recirculation and vice versa. Following Oldroyd (1965), C can be written as

$$C=\nabla M\times\nabla w, \tag{15}$$

where M is defined as

$$M=\nabla\cdot(\Psi_2(\dot\gamma)\,\nabla w). \tag{16}$$

We further define the ratio $\theta(\dot\gamma)=\Psi_2(\dot\gamma)/\eta_s(\dot\gamma)$, and write

$$M=\theta(\dot\gamma)p_z+\eta_s(\dot\gamma)\theta'(\dot\gamma)\,\nabla\dot\gamma\cdot\nabla w, \tag{17}$$

where the prime $'$ denotes derivative and $\nabla\cdot(\eta_s(\dot\gamma)\nabla w)$ has been replaced by the constant p_z by virtue of Eq. (14). Equation (17) suggests two sufficient conditions for rectilinear flows in the pipe (that is, without secondary recirculation). One is $\theta'(\dot\gamma)=0$, which is Oldroyd's condition of Ψ_2 being a constant multiple of η_s. The other is an axisymmetric cross section such as a circle or a circular annulus, in which M is a sole function of $\dot\gamma$ and ∇M, $\nabla\dot\gamma$, and ∇w are all collinear along the radial direction.

It turns out that the behavior of M can be inferred from the first term on the right hand side of the preceding equation: $M_1=\theta(\dot\gamma)p_z$, and that of C from

$$C_1=\nabla M_1\times\nabla w=p_z\theta'(\dot\gamma)\,\nabla\dot\gamma\times\nabla w. \tag{18}$$

First, consider a cross section that only deviates slightly from circular, with radial coordinate r. Then $\dot\gamma=|\nabla w|\approx -w'(r)$, and $\nabla\dot\gamma$ is nearly parallel to ∇w everywhere. Now the second term of M can be estimated as

$$M_2=\eta_s\theta'\,\nabla\dot\gamma\cdot\nabla w\approx\eta_s\theta'(-w'w'')\approx\eta_s\theta'\dot\gamma\nabla^2 w. \tag{19}$$

If we further assume the weak flow condition ($De\ll 1$), η_s may be taken to be constant, and θ can be linearized as $\theta(\dot\gamma)=\theta_0+\theta'(\dot\gamma)\dot\gamma$, θ_0 being a constant. Now M_2 becomes

$$M_2=\eta_s[\theta(\dot\gamma)-\theta_0]\nabla^2 w\approx[\theta(\dot\gamma)-\theta_0]\,\nabla\cdot(\eta_s\nabla w)=M_1-p_z\theta_0. \tag{20}$$

Thus, in the double limit of slow flow and near-circular cross section, M_2 is equal to M_1 minus the constant $\theta_0 p_z$, and the curl of the viscoelastic body force becomes

$$C=C_1+C_2=2C_1. \tag{21}$$

In the general case, the equalities in Eqs. (19) and (20) no longer hold. But a scaling argument based on $\dot\gamma=|\nabla w|\sim W/D$ and $\theta'\sim\theta D/W$ will still show M_1 and M_2, and consequently C_1 and C_2, to be on the same order of magnitude. This implies that instead of C, we can study the relatively simple C_1 as the driving force of secondary flows.

Figure 6 provides empirical evidence for the correspondence between C and C_1. From contours of w and $\dot\gamma$ in the square cross section [Figs. 6(a) and 6(b)], it is apparent that $\nabla\dot\gamma$ and ∇w are no longer parallel in the noncircular geometry. Their cross product $\nabla\dot\gamma\times\nabla w$, as appears in C_1, is illustrated in (c), while (d) plots C calculated directly from the polymer stresses in the finite element solution. Plot (c) displays a clear division of opposite signs by the diagonal: $\nabla\dot\gamma\times\nabla w>0$ above the diagonal and $\nabla\dot\gamma\times\nabla w<0$ below. From Fig. 4(b), which plots a normalized $-\theta$ against De, the Giesekus model has θ as an increasing function of the shear rate: $\theta'(\dot\gamma)>0$ for all $\dot\gamma$. With $p_z<0$, Eq. (18) gives a negative C_1 above the diagonal and a positive C_1 below. Thus, C_1 and C have the same signs and similar contour patterns. Moreover, the magnitudes of those two have a close correspondence. For example, at the point where the $\dot\gamma=5$ contour intersects the upper

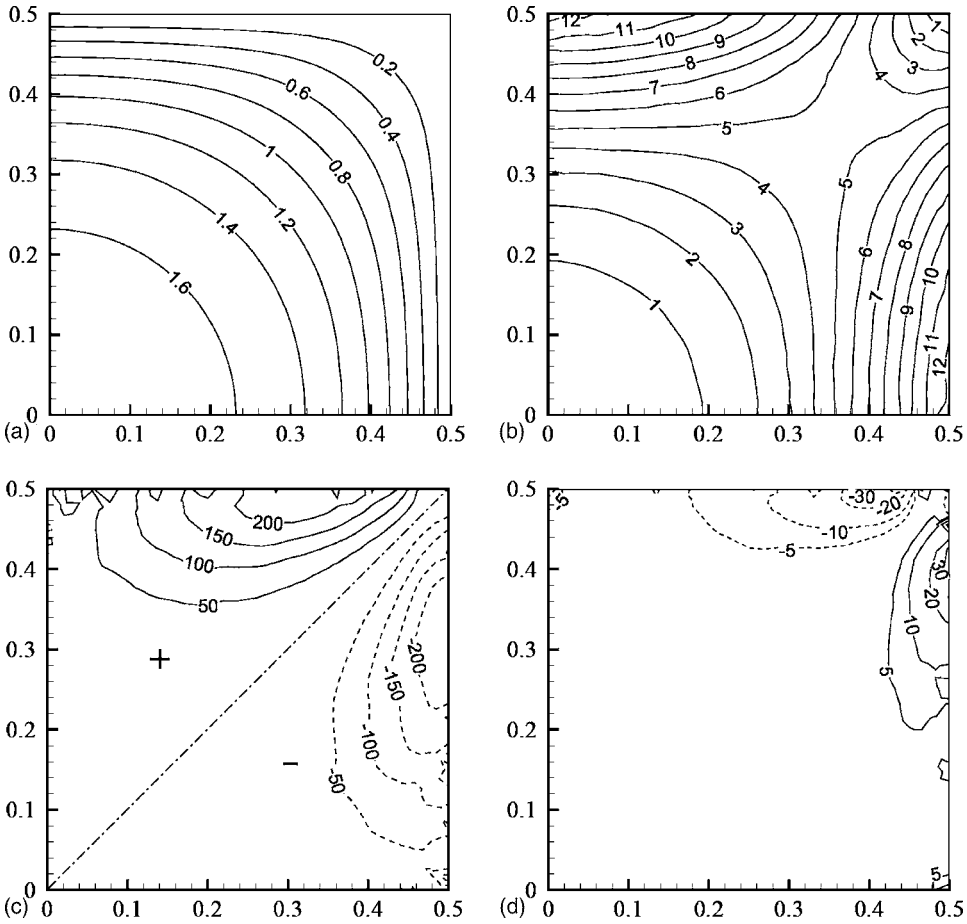

FIG. 6. Kinematics and dynamics of the secondary flow in the square cross section at $De=1$, $\alpha=0.5$, $\beta=0.1$, and $p_z=-6.78$. (a) Contours of the axial velocity w; (b) contours of the shear rate $\dot{\gamma}$; (c) contours of $\nabla\dot{\gamma}\times\nabla w$; (d) contours of the curl of extra body force: $C=\nabla\times\boldsymbol{f}$. The numerical noise near the walls in (c) and (d) arises from differentiating the velocity and stress fields twice.

wall [$x\approx0.39$ in Fig. 6(b)], $\nabla\dot{\gamma}\times\nabla w\approx200$ in Fig. 6(c). From Fig. 4(b), the corresponding $\theta'(\dot{\gamma})$ reads about 0.018 after accounting for the normalizing factors. Along with $p_z=-6.78$, this gives $C_1\approx-24$, close to $C\approx-30$ in Fig. 6(d). Therefore, although we do not have a mathematical proof for the relationship between C_1 and C beyond the limiting conditions of slow flow and near-circular cross sections, the former does seem to be a reliable indication of the latter, and consequently of the direction of the secondary flow.

Indeed, Fig. 6 highlights $\theta'(\dot{\gamma})$ as the key to the secondary flow. Since $\nabla\dot{\gamma}\times\nabla w$ depends mainly on the cross-sectional shape, its contour pattern is a robust kinematic feature insensitive to fluid rheology. It is $\theta'(\dot{\gamma})$ that determines the direction of viscoelastic forcing in the cross-sectional plane. Based on the previous analysis, we propose the following criterion on the direction of the secondary recirculation: if $\theta'(\dot{\gamma})>0$, the fluid flows along the side wall toward the corner and then inward toward the tube center, as is usually seen experimentally; if $\theta'(\dot{\gamma})<0$, the secondary flow will be in the opposite direction. Note that the criterion holds for $p_z<0$ as well as $p_z>0$. The sense of the recirculation depends on the sign of C, which is, however, independent of the sign of p_z

TABLE I. A summary of prior computations of the viscoelastic secondary flow in a square pipe. The last column indicates the direction of the secondary flow.

Reference	Constitutive model	$\Psi_2(\dot{\gamma})$	$\eta_s(\dot{\gamma})$	$\theta'(\dot{\gamma})$	Toward corner?
Green and Rivlin (1956)	Reiner–Rivlin	$\Psi_2'>0$	$\eta_s'=0$	>0	Yes
Gao and Hartnett (1993)	Reiner–Rivlin	$\Psi_2=0.0031$[a]	$\eta_s\propto\dot{\gamma}^{n-1}$,	>0	Yes
		$\Psi_2=-0.0031$	$n=0.7$	<0	No
Hashemabadi and Etemad (2006)	Reiner–Rivlin	$\Psi_2=0.01$[a]	$\eta_s\propto\dot{\gamma}^{n-1}$, $n=0.8$	>0	Yes
Dodson *et al.* (1974)	CEF	$\Psi_2>0$, $\Psi_2'=0$	$\eta_s'<0$	>0	Yes
Townsend *et al.* (1976)	CEF	$\Psi_2=0.001-k\eta_s$[b]	$\eta_s'<0$	>0	Yes
Mai–Duy and Tanner (2005)	CEF	$\Psi_2=c\dot{\gamma}^m$ [c]	$\eta_s\propto\dot{\gamma}^{n-1}$	>0	Yes
Syrjälä (1998)	CEF	$\Psi_2=c\dot{\gamma}^n$	$\eta_s\propto\dot{\gamma}^{n-1}$	>0	Yes
				<0	No
Xue *et al.* (1995)	MPTT	$\Psi_2<0$	$\eta_s'<0$	>0	Yes
Tanoue *et al.* (2006)	PTT	$\Psi_2<0$	$\eta_s'<0$	>0	Yes
Debbaut and Dooley (1999)	Giesekus[d]	$\Psi_2<0$	$\eta_s'<0$	>0	Yes
Siline and Leonov (2001)	Leonov[d]	$\Psi_2<0$	$\eta_s'<0$	>0	Yes

[a]No units were given for Ψ_2 in Gao and Hartnett (1993); Hashemabadi and Etemad (2006).
[b]Ψ_2, k and η_s are in cgs units, with two values of k: $k=0.004$ and 0.0015.
[c]$c<0$, $m=-1.35$, $n=0.37$.
[d]The analytical formulas for N_2 and η_s are given in Isaki and Takahashi (2002).

because changing the sign of p_z is accompanied by changing the sign of ∇w. In light of the previous analysis, the fallacy of the "intuitive" argument given at the end of the last subsection lies in taking N_2 as the driving force for the recirculation, whereas in reality, it is C.

All prior computational results are consistent with the θ' criterion, as is summarized in Table I. The table includes all the studies that we have found in the literature, with three exceptions. Wheeler and Wissler (1966) showed a plot of the recirculating streamlines but gave no information on the rheological parameters. It is then impossible to determine whether their result conforms to our criterion. Thangam and Speziale (1987) predicted secondary flows using a corotational Maxwell model, even though Ψ_2/η_s is a constant. This violates Oldroyd's condition and may be in error. Gervang and Larsen (1991) seem to have mispresented their data because of conflicting sign conventions in the stress tensor, and the correct result was later produced by Mai–Duy and Tanner (2005) using exactly the same model and parameters. In particular, this criterion reconciles previous computations using constitutive models with various forms of Ψ_2, and in effect generalizes Syrjälä's criterion [Syrjälä (1998)] to one apparently applicable to all viscoelastic models. Thus, one is tempted to term it a "universal criterion". However we have to remind the reader that the criterion has been derived by approximating the second term in Eq. (17) based on asymptotic limits and a scaling argument. This seems to be a reasonable assumption for all the popular models and is supported by our numerical results. Nonetheless, the claim to universality is subject to the theoretical possibility of a special fluid whose rheology upsets the approximation of M_2.

The criterion also seems consistent with experimental observations, although the scarcity of $N_2(\dot{\gamma})$ data precludes as detailed a comparison as provided in Table I. Because of the small magnitude of secondary flows, their visualization is no simple task [Tanner (2000)]. In all experiments to date [Dodson *et al.* (1974); Townsend *et al.* (1976); Debbaut *et al.* (1997); Dooley *et al.* (1998); Dooley (2002); Dooley and Rudolph (2003)], the

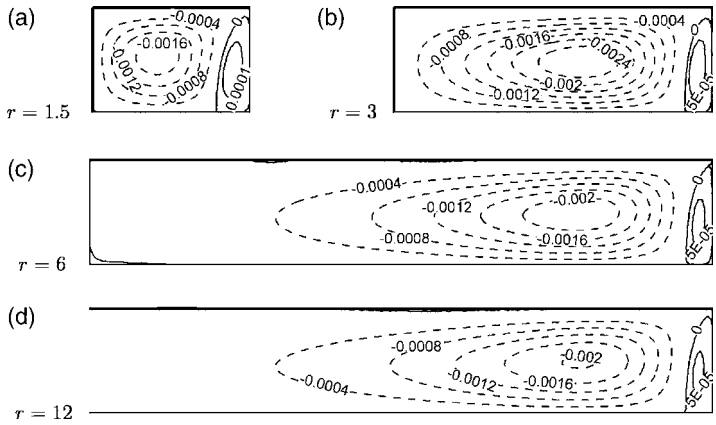

FIG. 7. Contours of the stream function ψ in rectangular cross sections with different aspect ratios r. Only the upper right quarter is shown. The length in the y direction is fixed to 1. De=1, α=0.5 and β=0.1.

secondary flow is from the center of side walls toward the corner. The experimental fluids include polyacrylamide, polyethylene oxide, polyisobutylene, and surfactant solutions [Dodson *et al.* (1974); Townsend *et al.* (1976)] and polystyrene and polyethylene melts [Debbaut *et al.* (1997); Dooley *et al.* (1998); Dooley (2002); Dooley and Rudolph (2003)]. Unfortunately, none of the authors provided $N_2(\dot{\gamma})$ or $\Psi_2(\dot{\gamma})$ data for the experimental fluids that would allow the evaluation of $\theta'(\dot{\gamma})$. From the literature we have found such data for fluids very similar to those used in the secondary flow experiments. For example, Christiansen and Leppard (1974) reported that for polyacrylamide and polyethylene oxide solutions, $N_2<0$, $-N_2 \propto \dot{\gamma}^n$ with $0<m<1$ and $\eta_s \propto \dot{\gamma}^n$ with $-0.8<n<-0.6$. This means $\theta'(\dot{\gamma})>0$ for these two polymer solutions. The cone-and-plate measurements of Alvarez *et al.* (1985) and rod-climbing measurements of Magda *et al.* (1991b) both suggest a positive $\theta'(\dot{\gamma})$ for polyisobutylene solutions. For a polystyrene melt, data by Schweizer *et al.* (2004) also indicate $\Psi_2<0$ and $\theta'(\dot{\gamma})>0$. Incidentally, certain polymer and surfactant solutions exhibit a Ψ_2 that is positive or changes sign with $\dot{\gamma}$ [Barnes *et al.* (1975); Bird *et al.* (1987); Magda *et al.* (1991a)]. Townsend *et al.* (1976) explored the implications of a positive Ψ_2 to the secondary flow via computations but apparently the secondary flow of such "exotic" fluids has not been subject to experimental observation.

C. Secondary flow in other cross sections

The insights on the direction and cause of the secondary flow are not specific to square ducts. When the cross section changes from square to rectangular, the two recirculating eddies in each quadrant lose symmetry, as shown in Fig. 7. If one measures the strength of the recirculation by the absolute value of the stream function ψ, the eddy adjacent to the longer edge grows in strength at the expense of the other, in qualitative agreement with previous computations based on the MPPT model [Xue *et al.* (1995)]. This is evidently because the primary flow produces stronger shear, and hence stronger polymer stresses, near the wide sides than the narrow sides. If we take the height of the cross section as the characteristic length D, and increase its width (or aspect ratio r) while keeping all the other conditions unchanged, the size of the major eddy expands with r until $r \approx 6$ [Figs. 7(a)–7(c)]. For even wider cross sections ($r>6$), the two vortices

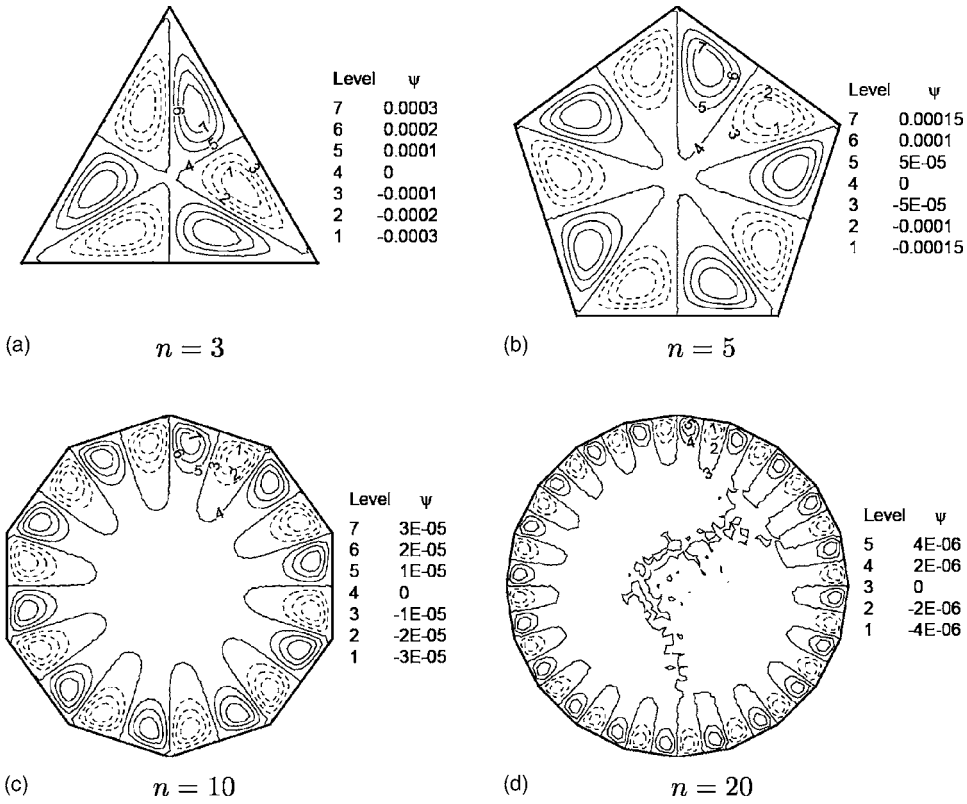

FIG. 8. The stream function for secondary flows in normal n-polygonal cross sections. The polygons have a common circumcircle of diameter 1. De=1, α=0.5, β=0.1. The wiggles in the central area of (d) are a numerical artifact in contouring small ψ values.

saturate in size, leaving a "dead water" zone at the channel center without secondary flow. This dead water zone may be beneficial to maintaining layer uniformity in coextrusion from dies of large aspect ratio, as occurs in film extrusion.

We did further calculations in normal polygons, as shown in Fig. 8. In all the cases, fluid flows from the center of the edges toward the corners, as in the square duct of Fig. 2. This is expected since the kinematic features inside the corners in Fig. 6 hold here as well. Due to symmetry, each edge accommodates two counter-rotating vortices. With the increase of edge number, the strength of secondary flow decreases and the dead water zone in the tube center expands. From the equilateral triangle [Fig. 8(a)] to the normal icosagon [Fig. 8(d)], the maximum ψ drops by two orders of magnitude. This is consistent with our argument based on C_1 as $\nabla\dot{\gamma}\times\nabla w$ is only nonzero in a small region near the corner. This region shrinks progressively as the angle between adjacent edges increases toward 180°. Obviously, the secondary flow will completely disappear when the cross section becomes circular.

Figure 9 shows the flow pattern in an elliptic cross section. Along the channel wall, fluid flows from the tip of the minor axis to the tip of the major axis where the shear rate is lower. The flow pattern agrees with the prediction of Green and Rivlin (1956) using the Reiner–Rivlin model, and is consistent with the arguments advanced in the square cross section. In fact, the tip of the major axis may be likened to a "corner", and the elliptic cross section to a "polygon" with two corners and two sides.

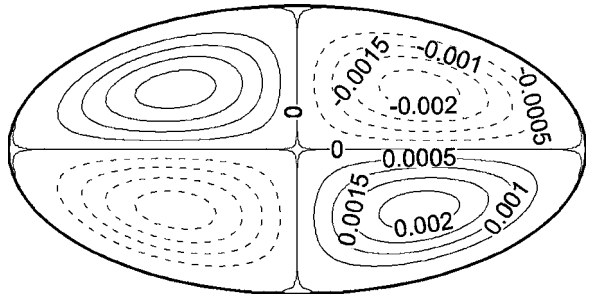

FIG. 9. The stream function in an elliptic cross section with major and minor axes of 2 and 1. $De=1$, $\alpha=0.5$ and $\beta=0.1$.

The final geometry to be considered is the annulus between a pair of slightly eccentric circular cylinders, through which a constant pressure gradient drives the axial primary flow. The diameters of the inner and outer cylinders are D and $2D$, respectively. The center of the inner cylinder is raised $0.05D$ from that of the outer cylinder, producing a small eccentricity that makes viscoelastic secondary flow possible. Figure 10 depicts the primary and secondary flows in the annulus. In the right half of the annulus, a clockwise recirculation occurs in the inner half of the gap, while a counterclockwise one, of weaker strength, prevails in the outer half. This picture is qualitatively the same as that predicted by Mollica and Rajagopal (1999) using a third-order fluid model.

This secondary flow can be analyzed by the same argument based on $C_1=p_z\theta'\nabla\dot{\gamma}\times\nabla w$. The axial velocity w is higher in the wider gap at the bottom than in the narrower gap on top. Near the cylinder walls, the flow is viscometric and ∇w is roughly normal to these boundaries. In the center of the gap, however, ∇w is smaller and along the azimuthal direction [Fig. 10(a)]. The shear rate $\dot{\gamma}$ is lower in the narrower upper part of the

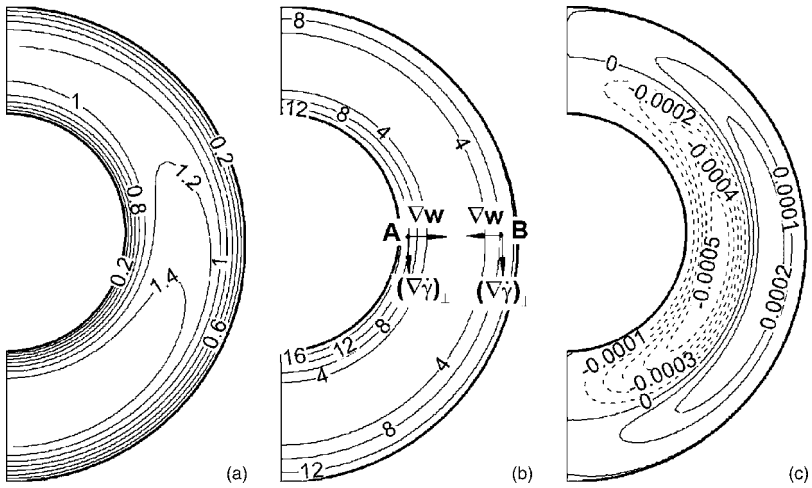

FIG. 10. The primary and secondary flows in the annulus between two slightly eccentric cylinders. Because of symmetry, only the right half of the cross section is shown. (a) Contours of the axial velocity w, (b) contours of the shear rate $\dot{\gamma}$, and (c) contours of the stream function ψ for the secondary flow. Judging from the ψ values, the outer eddy (solid lines) has about half the strength of the inner one (dashed lines). $De=1$, $\alpha=0.5$, $\beta=0.1$.

annulus than in the wider lower part. Thus, although the $\dot{\gamma}$ contours in Fig. 10(b) are nearly concentric arcs, $\nabla\dot{\gamma}$ does have a component $(\nabla\dot{\gamma})_\perp$ normal to ∇w, which points downward, as shown in the plot. Therefore, $\nabla\dot{\gamma}\times\nabla w$ is positive at point A near the inner cylinder and negative at B. As $p_z<0$ by convention and $\theta'>0$ in our Giesekus fluid, a negative C_1 prevails at A, producing a clockwise recirculation, and the opposite is true at B. Along either wall, the secondary flow goes from areas of high $\dot{\gamma}$ (bottom) toward areas of low $\dot{\gamma}$ (top). In this sense, the top corresponds to the corner of Fig. 6 and the bottom to the "center of the sides". As a matter of fact, one may generalize the criterion as follows so as to account for more general geometries: if $\theta'(\dot{\gamma})>0$, the secondary flow goes along solid walls from regions of high shear to low shear and then inward toward the center of the flow area; if $\theta'(\dot{\gamma})<0$, the secondary flow will be in the opposite direction.

IV. CONCLUSION

We have conducted theoretical analysis and numerical simulations on viscoelastic secondary flows in pipes of noncircular cross sections. We confirm that the second normal stress difference N_2 is the ultimate cause of secondary flows. However, the connection between N_2 and the direction of the secondary flow is subtler than often presumed in the literature. The main contribution of this study is to clarify that relationship. There are two main results:

1. A clear understanding of the mechanism for the secondary flow. The secondary recirculation is driven not by N_2 directly, but by the curl of an effective "body force" arising from N_2. For this body force to be nonconservative, two conditions have to be satisfied: the rheology must be such that the second normal stress coefficient is not a constant multiple of the shear viscosity, and the cross-section geometry is not axisymmetric.
2. A general criterion on the direction of the secondary flow, based on the ratio between the second normal stress coefficient and the shear viscosity $\theta(\dot{\gamma})=\Psi_2(\dot{\gamma})/\eta_s(\dot{\gamma})$. If $\theta(\dot{\gamma})$ is an increasing function of $\dot{\gamma}$, i.e., $\theta'(\dot{\gamma})>0$, the secondary flow is such as to go along the wall from regions of high shear to regions of low shear. In polygonal cross sections, the flow is from the center of the sides toward the corners. If $\theta'(\dot{\gamma})<0$, the secondary flow will be in the opposite direction.

We have compared our results with previous numerical and experimental studies. The criterion accounts for all previous computations and resolves apparent inconsistencies in the literature. Prior experimental observations, in pipes of square, rectangular, elliptic, and triangular cross sections, show the secondary flow to go from high shear regions to low shear regions along the wall. This is consistent with our criterion as available data suggest $\theta'(\dot{\gamma})>0$ for the polymer solutions and melts used. But the criterion is more than a summary of known results; it will be useful in predicting secondary flows in more complex die geometries and rheologically complex fluids. The eccentric annulus computed here may be considered an example of complex geometry, but polymer extrusion involves much more complex dies [Dooley *et al.* (1998); Dooley (2002)]. Regarding novel rheology, a host of complex fluids show unusual normal stress differences, including flexible polymer solutions, liquid crystalline polymers and surfactant solutions [Barnes *et al.* (1975); Bird *et al.* (1987); Magda *et al.* (1991a)]. Secondary flows in such fluids, as well as in heterogeneous systems (suspensions, emulsions, and foams), remain open questions.

ACKNOWLEDGMENTS

This work was supported by the NSERC, the Canada Research Chair program, the Canada Foundation for Innovation, and the NSFC (Grant No. 50390095).

APPENDIX

In the literature, secondary flows of a non-Newtonian fluid in a noncircular pipe are always attributed to the second normal stress difference N_2. We have never seen an explicit justification for this, and thus offer the following simple proof.

For an arbitrary point in the pipe, let us denote the primary flow direction by subscript 1, and the local velocity gradient and neutral directions by subscripts 2 and 3. The total stress tensor at that point is

$$\boldsymbol{\sigma} = -p\boldsymbol{I} + \begin{pmatrix} \tau_{11} & \tau_{12} & \tau_{13} \\ \tau_{12} & \tau_{22} & \tau_{23} \\ \tau_{13} & \tau_{23} & \tau_{33} \end{pmatrix} = -\bar{p}\boldsymbol{I} + \begin{pmatrix} N_1 + N_2 & \tau_{12} & 0 \\ \tau_{12} & N_2 & 0 \\ 0 & 0 & 0 \end{pmatrix}, \tag{A1}$$

where $\bar{p} = p - \tau_{33}$. In a fully developed pipe flow driven by a constant pressure gradient p_1, the modified pressure can be written as $\bar{p} = \tilde{p}(x_2, x_3) + p_1 x_1$, and the other variables satisfy $\partial / \partial x_1 = 0$. Now the momentum equations in directions 2 and 3 can be written as

$$\rho\left(\frac{\partial u_2}{\partial t} + u_2\frac{\partial u_2}{\partial x_2} + u_3\frac{\partial u_2}{\partial x_3}\right) = -\frac{\partial \tilde{p}}{\partial x_2} + \frac{\partial N_2}{\partial x_2}, \tag{A2}$$

$$\rho\left(\frac{\partial u_3}{\partial t} + u_2\frac{\partial u_3}{\partial x_2} + u_3\frac{\partial u_3}{\partial x_3}\right) = -\frac{\partial \tilde{p}}{\partial x_3}, \tag{A3}$$

and the continuity equation is reduced to

$$\frac{\partial u_2}{\partial x_2} + \frac{\partial u_3}{\partial x_3} = 0, \tag{A4}$$

which determines the pressure $\tilde{p}$ as a Lagrange multiplier. Then it becomes obvious that N_1 does not enter the governing equations of u_2 and u_3 and any secondary flow must be due to N_2.

References

Alvarez, G. A., A. S. Lodge, and H.-J. Cantow, "Measurement of the first and second normal stress differences: Correlation of four experiments on a polyisobutylene/decalin solution 'D1'," Rheol. Acta **24**, 368–376 (1985).

Barnes, H. A., A. R. Eastwood, and B. Yates, "A comparison of the rheology of two polymeric and two micellar systems. Part II: Second normal stress difference," Rheol. Acta **14**, 61–70 (1975).

Bird, R. B., R. C. Armstrong, and O. Hassager, *Dynamics of Polymeric Liquids, Vol. 1. Fluid Mechanics* (Wiley, New York, 1987).

Christiansen, E. B., and W. R. Leppard, "Steady-state and oscillatory flow properties of polymer solutions," Trans. Soc. Rheol. **18**, 65–86 (1974).

Debbaut, B., T. Avalosse, J. Dooley, and K. Hughes, "On the development of secondary motions in straight channels induced by the second normal stress difference: experiments and simulations," J. Non-Newtonian Fluid Mech. **69**, 255–271 (1997).

Debbaut, B., and J. Dooley, "Secondary motions in straight and tapered channels: Experiments and three-dimensional finite element simulation with a multimode differential viscoelastic model," J. Rheol. **43**, 1525–1545 (1999).

Dodson, A. G., P. Townsend, and K. Walters, "Non-Newtonian flow in pipes of non-circular cross section," Comput. Fluids **2**, 317–338 (1974).

Dooley, J., "Viscoelastic flow effects in multi-layer polymer coextrusion," Ph. D. thesis, Eindhoven University of Technology, Eindhoven, The Netherlands, 2002.

Dooley, J., K. S. Hyun, and K. Hughes, "An experimental study on the effect of polymer viscoelasticity on layer rearrangement in coextruded structures," Polym. Eng. Sci. **38**, 1060–1071 (1998).

Dooley, J., and L. Rudolph, "Viscous and elastic effects in polymer coextrusion," J. Plast. Film Sheeting **19**, 111–122 (2003).

Gao, S. X., and J. P. Hartnett, "Steady flow of non-Newtonian fluids through rectangular ducts," Int. Commun. Heat Mass Transfer **20**, 197–210 (1993).

Gao, S. X., and J. P. Hartnett, "Heat transfer behavior of reiner-rivlin fluids in rectangular ducts," Int. J. Heat Mass Transfer **39**, 1317–1324 (1996).

Gervang, B., and P. S. Larsen, "Secondary flows in straight ducts of rectangular cross section," J. Non-Newtonian Fluid Mech. **39**, 217–237 (1991).

Giesekus, H., "Sekundärströmungen in viskoelastischen Flüssigkeiten bei stationärer und periodischer Bewegung," Rheol. Acta **4**, 85–101 (1965).

Green, A. E., and R. S. Rivlin, "Steady flow of non-Newtonian fluids through tubes," Q. Appl. Math. **14**, 299–308 (1956).

Hashemabadi, S. H., and S. G. Etemad, "Effect of rounded corners on the secondary flow of viscoelastic fluids through non-circular ducts," Int. J. Heat Mass Transfer **49**, 1986–1990 (2006).

Isaki, T., and M. Takahashi, "Normal stress ratio predicted by viscoelastic vonstitutive equations," J. Soc. Rheol., Jpn. **30**, 65–69 (2002).

Magda, J. J., S. G. Baek, K. L. DeVries, and R. G. Larson, "Shear flow of liquid crystal polymers: Measurements of the second normal stress difference and the Doi molecular theory," Macromolecules **24**, 4460–4468 (1991a).

Magda, J. J., J. Lou, S. G. Baek, and K. L. DeVries, "Second normal stress difference of a Boger fluid," Polymer **32**, 2000–2009 (1991b).

Mai–Duy, N., and R. I. Tanner, "Computing non-Newtonian fluid flow with radial basis function networks," Int. J. Numer. Methods Fluids **48**, 1309–1336 (2005).

Mollica, F., and K. R. Rajagopal, "Secondary flows due to axial shearing of a third grade fluid between two eccentrically placed cylinders," Int. J. Eng. Sci. **37**, 411–429 (1999).

Oldroyd, J. G., "Some steady flows of the general elastico-viscous liquid," Proc. R. Soc. London, Ser. A **283**, 115–133 (1965).

Schweizer, T., J. van Meerveld, and H. C. Öttinger, "Nonlinear shear rheology of polystyrene melt with narrow molecular weight distribution—Experiment and theory," J. Rheol. **48**, 1345–1363 (2004).

Siline, M., and A. I. Leonov, "On flows of viscoelastic liquids in long channels and dies," Int. J. Eng. Sci. **39**, 415–437 (2001).

Syrjälä, S., "Laminar flow of viscoelastic fluids in rectangular ducts with heat transfer: A finite element analysis," Int. Commun. Heat Mass Transfer **25**, 191–204 (1998).

Tanner, R. I., *Engineering Rheology* (Oxford, New York, 2000).

Tanoue, S., T. Naganawa, and Y. Iemoto, "Quasi-three-dimensional simulation of viscoelastic flow through a straight channel with a square cross section," J. Soc. Rheol., Jpn. **34**, 105–113 (2006).

Thangam, S., and C. G. Speziale, "Non-Newtonian secondary flows in ducts of rectangular cross-section," Acta Mech. **68**, 121–138 (1987).

Townsend, P., K. Walters, and W. M. Waterhouse, "Secondary flows in pipes of square cross-section and measurement of the second normal stress difference," J. Non-Newtonian Fluid Mech. **1**, 107–123 (1976).

Wheeler, J. A., and E. H. Wissler, "Steady flow of non-Newtonian fluids in a square duct," Trans. Soc. Rheol. **10**, 353–367 (1966).

Xue, S.-C., N. Phan–Thien, and R. I. Tanner, "Numerical study of secondary flows of viscoelastic fluid in

straight pipes by an implicit finite volume method," J. Non-Newtonian Fluid Mech. **59**, 191–213 (1995).

Yue, P., C. Zhou, and J. J. Feng, "A computational study of the coalescence between a drop and an interface in Newtonian and viscoelastic fluids," Phys. Fluids **18**, 102102 (2006a).

Yue, P., C. Zhou, J. J. Feng, C. F. Ollivier–Gooch, and H. H. Hu, "Phase-field simulations of interfacial dynamics in viscoelastic fluids using finite elements with adaptive meshing," J. Comput. Phys. **219**, 47–67 (2006b).